A Modified Multi-innovation Algorithm to Turntable Servo System Identification

Linwei Li[1] · Huanlong Zhang[1] · Xuemei Ren[2]

Abstract

This paper is concerned with the identification of turntable servo system through the usage of a reframed multi-innovation least-squares scheme. A Wiener–Hammerstein model is employed in this paper to depict the dynamic characteristics of the turntable system. In the test bed, the stabilized platform can be considered as a linear dynamic subsystem. The motor is also a linear dynamic subsystem. And the major nonlinearity characteristic between motor and platform is captured by a continuously differentiable friction model. A new reframed multi-innovation least-squares approach (RMILS) is proposed to identify the Wiener–Hammerstein model. By introducing the intermediary step updating, the innovation updating is decomposed into sub-innovations updating, which can solve the inverse of covariance matrix and improve the identification performance. Then, the consistency nature of the RMILS method is discussed by using the theoretical analysis. Finally, the simulation and experiment results explain that the developed approach produces an outstanding performance in convergence speed and identification precision comparing to the conventional multi-innovation least-squares approach.

✉ Huanlong Zhang
  lgz20180514yfy@foxmail.com

  Linwei Li
  limengrui198801@163.com

  Xuemei Ren
  xmren@bit.edu.cn

[1] School of Electrical and Information Engineering, Zhengzhou University of Light Industry, Zhengzhou 450000, People's Republic of China

[2] School of Automation, Beijing Institute of Technology, Beijing 100081, People's Republic of China

Birkhäuser

1 Introduction

In recent decades, parameter identification techniques have attracted extensive interest in system modeling, signal processing, control system design and fault diagnosis, etc. [5,18,24,34]. In system modeling, block-oriented models (B-O-M) have become one of the popular nonlinear modeling approaches because of their advantages to capture the behavior of the practical system, and to provide a model analysis for control system. On the other hand, B-O-M consist of interaction of linear dynamic submodels and static nonlinear submodels. Such combination characteristic is flexible to use and easy to understand. By far the simplest and most widely used combination models are Hammerstein (for short, H-S) and Wiener systems (W-S). The extension versions involve Wiener–Hammerstein (for short, W–H-S) and Hammerstein–Wiener systems (H–W-S). The extended systems can provide higher modeling capabilities than the H-S and W-S. In this paper, the focus is made on the identification and system modeling of the W–H-S as depicted in Fig. 1, where L_1 is the first subsystem, the middle friction nonlinearity is denoted by $f(\cdot)$, and the third subsystem is L_2.

Many efforts have been made on the parameter identification and system modeling of W–H-S [6,11,20,26,30]. Giordano et al. [6] developed a modified fractional approach to divide the poles and zeros for two linear subsystems of W–H-S by transforming discrete problem into continuous problem way, and estimated initial value of systems based on the best linear approximation method and Newton algorithm. Mzyk et al. [20] utilized a kernel-type nonparametric estimate to estimate static nonlinear part of W–H-S and used kernel-correlation estimator to identify the linear dynamic characteristic. Dong et al. [2] applied two-step estimation method to obtain the parameter information for the micro-positioning stage with piezoelectric actuator based on the W–H-S with hysteresis nonlinearity. In Schoukens et al. [23], the W–H-S are approximated based on the best linear approximation technique, and the parameter of models are estimated by using the L–M approach. In some mild assumptions, the presented estimation schemes are effective. However, in aforementioned works, the W–H-S in which the middle nonlinear block is a linear combination of basis functions (e.g., [20,23,30]) or rational fraction function (e.g., [6]) is presented to model the practical system. When the practical system exhibits a strong nonlinear information, the W–H-S with a linear combination of basis function or rational fraction function may not effectively capture system dynamics or even may not be valid. Therefore, it is necessary to replace the above nonlinear block by using an appropriate nonlinear element when we model the complex nonlinear system such as the servo system and X–Y positioning table. In [32], a switched nonlinear autoregressive moving average eXogenous model developed by Zhang et al. is used to model the turntable servo system, in which system parameters are estimated by using the particle swarm optimization
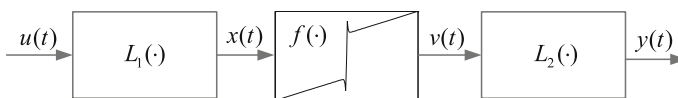

Fig. 1 Wiener–Hammerstein systems with friction

algorithm. A cascade model for the servo system is presented in the literature [31], in which the particle swarm optimization is used to identify the system parameter, the cross-validation shows that there is a good correspondence between the real equipment and the identified model. Na et al. [22] used an improved Lyapunov–Krasovskii functions to handle the unknown time-delays, and a novel high-order neural network model is used to model the unknown deadzone and others nonlinearities of robotic servo system. Finally, the tracking control is achieved by developing an adaptive controller. In the above literature, the modeling of servo system is based on the global approximation method, partial approximation method or simple cascade model, which may produce an unsatisfactory modeling performance due to the complex dynamic of servo system. Inspired by literature [2], the complex W–H-S model is used to model for servo system based on a novel friction submodel.

In recent years, the design and development of multi-innovation identification idea have been proven to be simple and effective in theory [17,25] and engineering application [14,33]. The basic idea of multi-innovation theory is to expand the scalar innovation into multi-innovation vector or matrix by using the several groups of data, to improve the utilization rate of estimator based on the current and past time system information, which can enhance the estimation accuracy and convergence speed of identification algorithm. Multi-innovation theory is a natural extension of scalar innovation, which only uses available system information and does not need an additional design to improve the identification performance. Inspired by the multi-innovation identification idea, a new reframed identification approach for the identification of Wiener–Hammerstein with friction and the modeling of the turntable servo system are designed by using the intermediary step updating. The major contributions of this paper are provided as follows:

(1) A new reframed multi-innovation least-squares scheme (RMILS) is proposed to solve the problem of multi-innovation length p in conventional MILS method by using the intermediary step updating. The multi-innovation update is transformed into p sub-innovations update, which effectively addresses inversion of covariance matrix. Moreover, the consistency proof of the presented estimator has indicated that the estimation value can converge to desired value.

(2) According to the nonlinear characteristic of turntable servo system, we choose the friction nonlinearity as nonlinear submodel rather than a linear combination of basis functions or rational fraction function, which is more suitable for modeling the turntable servo system.

(3) The efficacy and usefulness of the developed method is checked on the system identification and modeling of turntable servo system based on the W–H-S with frication nonlinearity. Numerical verification and experimental analyses are convincingness and rationality for using the algorithm presented in practice.

The remainder of this paper is given as follows. The W–H-S with friction is introduced in Sect. 2. Section 3 derives the RMILS approach. The convergence analysis of the proposed algorithm is given in Sect. 4. Section 5 provides the numerical example and experiment, and discussion is given in Sect. 6. Section 7 shows some conclusions.

2 System Description and Identification Model

The structure of the W–H-S with friction nonlinearity to model the turntable servo system is displayed in Fig. 1, where $u(t)$ and $y(t)$ denote the input–output of the system, $x(t)$, $v(t)$ are outputs of the linear subsystem (L_1) and friction. $d(t)$ represents the noise signal. L_1 and L_2 can be expressed as

$$x(t) = \sum_{i=1}^{n_a} a_i u(t-i) - \sum_{j=1}^{n_b} b_j x(t-j), \tag{1}$$

$$y(t) = \sum_{m=1}^{n_c} c_m v(t-m) - \sum_{n=1}^{n_d} d_n y(t-n) + d(t). \tag{2}$$

Assume that the linear dynamic subsystems L_1 and L_2 are stable, n_a, n_b, n_c and n_d are known. $a_1, \ldots, a_{n_a}$, $b_1, \ldots, b_{n_b}$, $c_1, \ldots, c_{n_c}$ and $d_1, \ldots, d_{n_d}$ are unknown, $u(t) = 0$, $x(t) = 0$, $v(t) = 0$ and $y(t) = 0$ for $t \le 0$. Let both $a_1 = 1$, $c_1 = 1$ for the unique description of identification model [3,12].

The identifications of discontinuous or piecewise continuous friction model parameters are time-consuming [1]. Moreover, these models may lead to a problematic for smooth control actions [21]. In this paper, a newly proposed continuously differentiable friction model [19,29] is applied, which is described by the following parameterized form:

$$v(t) = \gamma_1 \tanh(\gamma_2 \dot{x}(t)) - \gamma_1 \tanh(\gamma_3 \dot{x}(t)) + \gamma_4 \tanh(\gamma_5 \dot{x}(t)) + \gamma_6 \dot{x}(t), \tag{3}$$

where γ_i, $i = 1, 2, \ldots, 6$ represent positive parameters.

Compared with the mentioned friction model (e.g., Coulomb, LuGre and GMS), friction model (3) possesses a continuously differentiable form to enable more suitable parameter identification. It can capture the following major behavior discussed in friction modeling: (1) γ_1 and γ_4 denote the coefficient of the static friction. (2) $\tanh(\gamma_2 \dot{x}) - \tanh(\gamma_3 \dot{x})$ can capture the so-called Stribeck effect. (3) $\gamma_4 \tanh(\gamma_5 \dot{x})$ dominates the Coulomb friction. (4) The viscous dissipation term is given by $\gamma_6 \dot{x}$. For more information on friction model (3), the reader can refer to [19].

To achieve the system modeling of the turntable servo system, based on the property of function $\tanh(\cdot)$, the output and input characteristics of Eq. (3) can be described by the following equation:

$$v(t) = \gamma_6 x(t) - \gamma_6 x(t-1) + \beta_1 \text{sign}(x(t)-x(t-1)) - \beta_2 \tanh(x(t)-x(t-1)), \tag{4}$$

where β_1, β_2 are positive parameters, $\text{sign}(\cdot)$ denotes the sign function.

Substituting (1) and (4) into (2) and applying the key-term separation principle [27] yields

$$y(t) = c_1 \gamma_6 \sum_{i=1}^{n_a} a_i u(t-i-1) - c_1 \gamma_6 \sum_{j=1}^{n_b} b_j x(t-j-1) - c_1 \gamma_6 x(t-2)$$

$$+ c_1 \beta_1 \text{sign}(x(t-1) - x(t-2)) - c_1 \beta_2 \tanh(x(t-1) - x(t-2))$$

$$+ \sum_{m=2}^{n_c} c_m v(t-m) - \sum_{n=1}^{n_d} d_n y(t-n) + d(t). \tag{5}$$

In order to obtain the identification model, (5) can be equivalently written as

$$y(t) = \varphi^T(t)\theta + d(t), \tag{6}$$

where the data vector $\varphi(t)$ and the vector θ are listed as follows:

$$\varphi(t) = [u(t-2), u(t-3), \ldots, u(t-n_a-1), -x(t-2), -x(t-3), \ldots,$$
$$- x(t-n-b-1), \text{sign}(x(t-1) - x(t-2)), -\tanh(x(t-1) - x(t-2)),$$
$$v(t-2), v(t-3), \ldots, v(t-n_c), -y(t-1), -y(t-2), \ldots, -y(t-n_d)]^T,$$

and

$$\theta = [c_1 a_1 \gamma_6, \ldots, c_1 a_{n_a} \gamma_6, c_1 b_1 \gamma_6 + c_1 \gamma_6, c_1 b_2 \gamma_6, \ldots c_1 b_{n_b} \gamma_6, c_1 \beta_1, c_1 \beta_2,$$
$$c_2, c_3, \ldots, c_{n_c}, d_1, d_2, \ldots, d_{n_d}]^T,$$

where

$$\gamma_6 = c_1 a_1 \gamma_6, a_2 = c_1 a_2 \gamma_6 / \gamma_6, \ldots, \ a_{n_a} = c_1 a_{n_a} \gamma_6 / \gamma_6, b_1 = (c_1 b_1 \gamma_6 + c_1 \gamma_6) / \gamma_6 - 1,$$
$$b_2 = c_1 b_2 \gamma_6 / \gamma_6, \ldots, b_{n_b} = c_1 b_{n_b} \gamma_6 / \gamma_6, \beta_1 = c_1 \beta_1, \beta_2 = c_1 \beta_2.$$

3 Reframed Multi-innovation Least-Squares Algorithm

In the field of system identification, recursive least squares method (RLS) is one of the most popular identification algorithms [8,9]. The multi-innovation least-squares algorithm (MILS) is designed for the purpose of improving the convergence rate of the RLS [4,28]. To display the advantage of the RMILS, the MILS will be briefly introduced.

For the identification model (6), defining the criterion function $J(\theta) = [y(t) - \varphi^T(t)\theta]^2$ and minimizing the quadratic criterion $J(\theta)$, then we can get the RLS method, in which $e(t) = y(t) - \varphi^T(t)\hat{\theta}(t-1)$ represents the scalar innovation [10]. Expanding the scalar innovation $e(t)$ to the innovation vector (multi-innovation) $\mathbf{E}(p, t)$ by using newest p data: $\mathbf{Y}(p, t) = [y(t), y(t-1), \ldots, y(t-p+1)]^T$, $\mathbf{E}(p, t) = [e(t), e(t-1), \ldots, e(t-p+1)]^T$, $\phi^T(p, t) = [\varphi^T(t), \varphi^T(t-1), \ldots, \varphi^T(t-p+1)]^T$, where p represents the innovation length ($p \geq 1$).

Based on the innovation vector, MILS is written as follows:

$$\hat{\theta}(t) = \hat{\theta}(t-1) + L(t)[\mathbf{Y}(p, t) - \boldsymbol{\phi}^T(p, t)\hat{\theta}(t-1)], \tag{7}$$

$$L(t) = P(t-1)\boldsymbol{\phi}(p, t)[I_p + \boldsymbol{\phi}^T(p, t)P(t-1)\boldsymbol{\phi}(p, t)]^{-1}, \tag{8}$$

$$P(t) = P(t-1) - L(t)\boldsymbol{\phi}^T(p, t)P(t-1), P(0) = p_0 I. \tag{9}$$

Noting that (7), (8), and (9) involve the unknown variables $\varphi(t)$ in $\boldsymbol{\phi}(p, t)$, and $x(t-i)$, $v(t-i)$ in $\varphi(t)$, one solution is to reconstruct the auxiliary model through the usage of the auxiliary model method [15,16]. The basic idea of the auxiliary model method is to replace the unknown variable by using their estimated values, i.e., $x(t-i)$ is replaced by $\hat{x}(t-i)$, where $\hat{x}(t-i)$ is the estimate of $x(t-i)$. Then, the information vector $\varphi(t)$ in (6) is replaced by using $\hat{\varphi}(t)$ such that $\boldsymbol{\phi}(p, t)$ is also known.

In the MILS method, the inverse of the covariance matrix in Eq. (8) needs to be calculated, which leads to a large amount of computation and singular value phenomenon. To tackle the above problem, the multi-innovation updating is divided into p sub-innovations updating steps by introducing the intermediary step updating. Then, the covariance matrix is transformed into scalar operation, which decreases the computational burden of the algorithm and improves the identification performance of the method. The decomposition is described as follows.

When $i = 1, \ldots, p$, the matrix $[1 + \varphi^T(t, i) P_{i-1}(t)\varphi(t, i)]$ is transformed into scalar operation. To achieve this purpose, $y(t)$ and $\varphi(t)$ are modified to $y(t, i)$ and $\varphi(t, i)$, then the RMILS is written as follows:

$$\hat{\theta}_i(t) = \hat{\theta}_{i-1}(t) + L_i(t)e(t, i), \tag{10}$$

$$e(t, i) = y(t, i) - \varphi^T(t, i)\hat{\theta}_{i-1}(t), \tag{11}$$

$$L_i(t) = P_{i-1}(t)\varphi(t, i)[1 + \varphi^T(t, i) P_{i-1}(t)\varphi(t, i)]^{-1}, \tag{12}$$

$$P_i(t) = P_{i-1}(t) - L_i(t)\varphi^T(t, i) P_{i-1}(t), \tag{13}$$

$$P_0(t) = P_p(t-1), \ L_0(t) = L_p(t-1), \ \hat{\theta}_0(t) = \hat{\theta}_p(t-1). \tag{14}$$

Remark 1 Compared with the MILS method, the RMILS approach can exact the system information as far as possible by using p the sub-innovation update steps under the same conditions without computing the inverse of covariance, which effectively improves the performance of the parameter identification. In iterative algorithm [30], the estimated parameter is updated by using L sets of data each time, which is repeated k times. In presented method, the estimated parameter is updated by using a set of data each time, which is computed from 1 to p. For the same system, in general, the length of innovation p is much less than the iterative time k.

In Eqs. (10)–(14), i represents the sub-innovation updating step, and $\hat{\theta}_0(0) = I/p_0$. when $i = p$ holds, then the next updating will be started.

4 Convergence Analysis

In this section, the convergency of the RMILS scheme will be studied. Assume that $\{d(t), \mathscr{F}_t\}$ is a bounded martingale, in which the algebra sequence $\{\mathscr{F}_t\}$ is constituted by $\{d(t)\}$, and the noise $\{d(t)\}$ satisfies [7]

(A1) $E[d(t)|\mathscr{F}_{t-1}] = 0$, a.s.,
(A2) $E[\|d(t)\|^2|\mathscr{F}_{t-1}] = \sigma_d^2(t) \leq \sigma_d^2 < \infty$, a.s.,
(A3) $\limsup\limits_{t\to\infty} \dfrac{1}{t} \sum\limits_{i=1}^{t} \|d(i)\|^2 \leq \sigma_d^2 < \infty$, a.s..

Theorem 1 *For the system* (6) *and the RMILS algorithm* (10)–(14), *assume that the input $u(t)$ satisfies persistent excitation condition, such that, $\alpha I \leq 1/t \sum_{j=1}^{t} \sum_{i=1}^{p} \hat{\varphi}(j,i)\hat{\varphi}^T(j,i) \leq \beta I, t \geq t_0$ and (A1)–(A3) hold, then the parameter estimation $(\widetilde{\theta}(t) = \hat{\theta}_p(t) - \theta)$ converges to zero, i.e., $\lim_{t\to\infty} \|\hat{\theta}_p(t) - \theta\|^2 = 0$, a.s..*

Proof Define the parameter error vector $\widetilde{\theta}_i(t) = \hat{\theta}_i(t) - \theta$, $i = 1, 2, \ldots, p$. Then, subtracting θ both sides of (10), it yields

$$
\begin{aligned}
\widetilde{\theta}_i(t) &= \widetilde{\theta}_{i-1}(t) + P_i(t)\hat{\varphi}(t,i)[\varphi^T(t,i)\theta - \hat{\varphi}^T(t,i)\hat{\theta}_{i-1}(t)] + P_i(t)\hat{\varphi}(t,i)d(t,i) \\
&= \widetilde{\theta}_{i-1}(t) + P_i(t)\hat{\varphi}(t,i)\{-\hat{\varphi}^T(t,i)\widetilde{\theta}_{i-1}(t) + [\varphi(t,i) - \hat{\varphi}^T(t,i)]^T\theta + d(t,i)\} \\
&= \widetilde{\theta}_{i-1}(t) + P_i(t)\hat{\varphi}(t,i)[-\widetilde{y}(t,i) + \triangle(t) + d(t,i)],
\end{aligned}
\tag{15}
$$

where $\widetilde{y}(t,i) = \hat{\varphi}^T(t,i)\hat{\theta}_{i-1}(t) - \hat{\varphi}^T(t,i)\theta = \hat{\varphi}^T(t,i)\widetilde{\theta}_{i-1}(t)$, $\triangle(t) = [\varphi(t,i) - \hat{\varphi}^T(t,i)]^T\theta$.

Based on (15) and $P_i^{-1}(t) = P_{i-1}^{-1}(t) + \hat{\varphi}(t,i)\hat{\varphi}^T(t,i)$, we obtain

$$
\begin{aligned}
\widetilde{\theta}_i^T(t)P_i^{-1}(t)\widetilde{\theta}_i(t) &= \{\widetilde{\theta}_{i-1}(t) + P_i(t)\hat{\varphi}(t,i)[-\widetilde{y}(t,i) + \triangle(t) + d(t,i)]\}^T P_i^{-1}(t) \\
&\quad \times \{\widetilde{\theta}_{i-1}(t) + P_i(t)\hat{\varphi}(t,i)[-\widetilde{y}(t,i) + \triangle(t) + d(t,i)]\} \\
&= \widetilde{\theta}_{i-1}^T(t)[P_{i-1}^{-1}(t) + \hat{\varphi}(t,i)\hat{\varphi}^T(t,i)]\widetilde{\theta}_{i-1}(t) + 2\widetilde{y}(t,i)[-\widetilde{y}(t,i) \\
&\quad + \triangle(t) + d(t,i)] + \hat{\varphi}^T(t,i)P_i(t)\hat{\varphi}(t,i)[\widetilde{y}(t,i)^2 + d(t,i)^2 \\
&\quad + \triangle(t)^2 - 2\widetilde{y}(t,i)d(t,i) - 2\widetilde{y}(t,i)\triangle(t) + 2\triangle(t)d(t,i)] \\
&= \widetilde{\theta}_{i-1}^T(t)P_{i-1}^{-1}(t)\widetilde{\theta}_{i-1}(t) - [1 - \hat{\varphi}^T(t,i)P_i(t)\hat{\varphi}(t,i)]\widetilde{y}(t,i)^2 \\
&\quad + 2[1 - \hat{\varphi}^T(t,i)P_i(t)\hat{\varphi}(t,i)]\widetilde{y}(t,i)[\triangle(t) + d(t,i)] \\
&\quad + \hat{\varphi}^T(t,i)P_i(t)\hat{\varphi}(t,i) \times [d(t,i)^2 + \triangle(t)^2 + 2\triangle(t)d(t,i)].
\end{aligned}
\tag{16}
$$

Assume that $\{\triangle(t)\}$ is bounded, e.g., $\triangle(t)^2 \leq \varepsilon < \infty$. Since $\widetilde{\theta}_{i-1}^T(t)P_{i-1}^{-1}(t)\widetilde{\theta}_{i-1}(t)$, $\widetilde{y}(t,i)$, $\hat{\varphi}^T(t,i)P_i(t)\hat{\varphi}(t,i)$ and $\triangle(t)$ are uncorrelated with $d(t,i)$, and $1 - \hat{\varphi}^T(t,i)P_i(t)\hat{\varphi}(t,i) = [1 + \hat{\varphi}^T(t,i)P_{i-1}(t)\hat{\varphi}(t,i)]^{-1} \geq 0$. Define the function $W_i(t) = E[\widetilde{\theta}_i^T(t)P_i^{-1}(t)\widetilde{\theta}_i(t)]$, the conditional expectation is taken on both sides of (16) with respect to $\mathscr{F}_{t-1}$ and using Assumptions (A1)–(A3), we have

$$
W_i(t) \leq W_i(t-1) + E\{\hat{\varphi}^T(t,i)P_i(t)\hat{\varphi}(t,i)[d(t,i)^2 + \triangle(t)^2]\}.
\tag{17}
$$

Summing for $W_i(t)$ from $i = 1$ to $i = p$. From (17), we obtain

$$
\begin{aligned}
W_p(t) &\leq W_p(t-1) + \sum_{i=1}^{p} E\{\hat{\varphi}^T(t,i)P_i(t)\hat{\varphi}(t,i)[\sigma_v^2 + \varepsilon]\} \\
&\leq W_p(0) + E\left\{\sum_{i=1}^{p}\sum_{j=1}^{t} \hat{\varphi}^T(j,i)P_i(j)\hat{\varphi}(j,i)[\sigma_v^2 + \varepsilon]\right\}.
\end{aligned}
\tag{18}
$$

Since $P_{i-1}^{-1}(t) = P_i^{-1}(t) - \hat{\varphi}(t, i)\hat{\varphi}^T(t, i)$, we have

$$|P_{i-1}^{-1}(t)| = |P_i^{-1}(t)||I - P_i(t)\hat{\varphi}(t, i)\hat{\varphi}^T(t, i)|,$$

$$\hat{\varphi}^T(t, i)P_i(t)\hat{\varphi}(t, i) = \frac{|P_i^{-1}(t)| - |P_{i-1}^{-1}(t)|}{|P_i^{-1}(t)|} = \int_{P_i^{-1}(t-1)}^{P_i^{-1}(t)} \frac{\mathrm{d}x}{|P_i^{-1}(t)|}.$$

Replacing t with j, and summing for i from 1 to p yield

$$\sum_{i=1}^p \sum_{j=1}^t \hat{\varphi}^T(j, i)P_i(j)\hat{\varphi}(j, i) \leq \sum_{i=1}^p \int_{P_i^{-1}(0)}^{P_i^{-1}(t)} \frac{\mathrm{d}x}{x} = \sum_{i=1}^p [\ln|P_i^{-1}(t)| + n \ln p_0]. \tag{19}$$

Applying the persistent excitation condition $\alpha I \leq 1/t \sum_{i=1}^p \sum_{j=1}^t \hat{\varphi}(j, i)\hat{\varphi}^T(j, i) \leq \beta I$, $t \geq t_0$ to $P_i^{-1}(t) = \sum_{i=1}^p \sum_{j=1}^t \hat{\varphi}(j, i)\hat{\varphi}^T(j, i) + P_i^{-1}(0)$, substituting $|P_i^{-1}(t)|$ into (19), we have

$$\sum_{i=1}^p \sum_{j=1}^t \hat{\varphi}^T(j, i)P_i(j)\hat{\varphi}(j, i) = \sum_{i=1}^p [\ln|P_i^{-1}(t)| + n \ln p_0]$$

$$\leq pn \ln(\beta t + 1/p_0) + pn \ln p_0. \tag{20}$$

According to the definition of $W_i(t)$, we have

$$W_p(t) \geq p(\alpha t + 1/p_0)E[\|\tilde{\theta}(t)\|]^2. \tag{21}$$

Since $W_p(0) = E[\tilde{\theta}^T(0)P^{-1}(0)\tilde{\theta}(0)] = pn/p_0^2$, substituting (20), (21) into (18) yields

$$p(\alpha t + 1/p_0)E[\|\tilde{\theta}(t)\|]^2 \leq W_p(t)$$

$$\leq W_p(0) + E\left\{\sum_{i=1}^p \sum_{j=1}^t \hat{\varphi}^T(j, i)P_i(j)\hat{\varphi}(j, i)[\sigma_v^2 + \varepsilon]\right\}$$

$$\leq pn/p_0^2 + [pn \ln(\beta t + 1/p_0) + pn \ln p_0][\sigma_v^2 + \varepsilon]. \tag{22}$$

Taking the limits of both sides of (22) with t, we have

$$\lim_{t \to \infty} [\|\tilde{\theta}(t)\|]^2 \leq \lim_{t \to \infty} \frac{n/p_0^2 + [n \ln(\beta t + 1/p_0) + n \ln p_0][\sigma_v^2 + \varepsilon]}{(\alpha t + 1/p_0)} = 0.$$

Theorem 1 has been shown. $\square$

5 Illustrative Example and Application

5.1 Illustrative Example

Consider the following W–H-S with friction block:

$L_1 : x(t) = u(t-1) + 2.2u(t-2) - 1.0x(t-1) - 0.5x(t-2),$
$L_2 : y(t) = v(t-1) + 0.2v(t-2) - 0.15y(t-1) - 0.4y(t-2) + d(t),$
Friction: $v(t) = 0.05x(t) - 0.05x(t-1) + 0.7\text{sign}(x(t) - x(t-1)) - 0.2\tanh(x(t) - x(t-1)).$

As can be seen from the example considered above, the desired parameter values are $a1 = 1$, $a2 = 2.2$, $b1 = 1.0$, $b2 = 0.5$, $c1 = 1$, $c2 = 0.2$, $d1 = 0.15$, $d2 = 0.4$, $\gamma_6 = 0.05$, $\beta_1 = 0.7$, $\beta_2 = 0.2$. In the simulation, the input $u(t)$ is mean $\mu = 0$ and variance $\sigma^2 = 1$ persistent excitation signal. The white noise $d(t)$ is uncorrelated with input persistent excitation signal whose signal-to-noise ratio is SNR = 7.4620. The sample length is N = 1000, $p = 4$, the initial value is chosen as $\hat{\theta}(0) = \mathbf{1}_9/10^2$ ($\mathbf{1}$ represents the unit column vector).

Applying the MILS and RMILS algorithms to estimate the parameter value θ of the W–H-S with friction, the comparative parameter convergence histories by both identification approaches are, respectively, depicted in Fig. 2a–c. It can be observed that the estimated values with solid line quickly tend to their expected value with dashed black line during the samples from 0 to 500, whereafter, the parameter estimation can reach their true values after about sample data 800. In order to reveal the evolutionary processes of the identification, the identification errors ($\delta = \|\hat{\theta}(t) - \theta\|/\|\theta\|$) by MILS algorithm with solid blue line and RMILS algorithm with solid red line are shown in Fig. 2d. It is shown that the estimation errors by both identification methods are rapidly decreasing in the initial stage of parameter estimation, and after the sample data 1000, the estimation errors tend to small steady value. The contrastive results shown in Fig. 2 indicate that the proposed algorithm (RMILS) provides a better estimation property both in the convergence speed and estimation precision compared to the MILS algorithm.

To test the results of parameter estimate, the contrastive modeling verifications are implemented based on the identification results, as shown in Fig. 3. The estimated model outputs by both algorithms with the dashed red line can capture the dynamics of the actual outputs with the solid blue line, which validates the usefulness of both algorithms. Compared with the MILS algorithm, the proposed algorithm produces an excellent predictive performance with a smaller model error.

The following indices are used to quantitatively analyze the capability of the estimator, in which the small indices mean the superiority of the estimator. (1) Normalized mean squared error (NMSE), NMSE $= \frac{1}{N'\sigma_y^2} \sum_{i=1}^{N'} (y_i - \hat{y}_i)^2$; (2) prediction error mean, $\mu_e = \frac{1}{N'} \sum_{i=1}^{N'} e_{\text{sim}}(t)$; (3) root mean square, $e_{RMSe} = \sqrt{\frac{1}{N'} \sum_{i=1}^{N'} e_{\text{sim}}(t)^2}$, where N' represents the sample length, σ_y^2 is the output variance and $e_{\text{sim}}(t) = y_t - \hat{y}_t$ is the error of prediction [19].

Based on the definition of μ_e, e_{RMSe} and NMSE, results of the performance indices are listed in Table 1. Table 1 displays the performance values of the identification

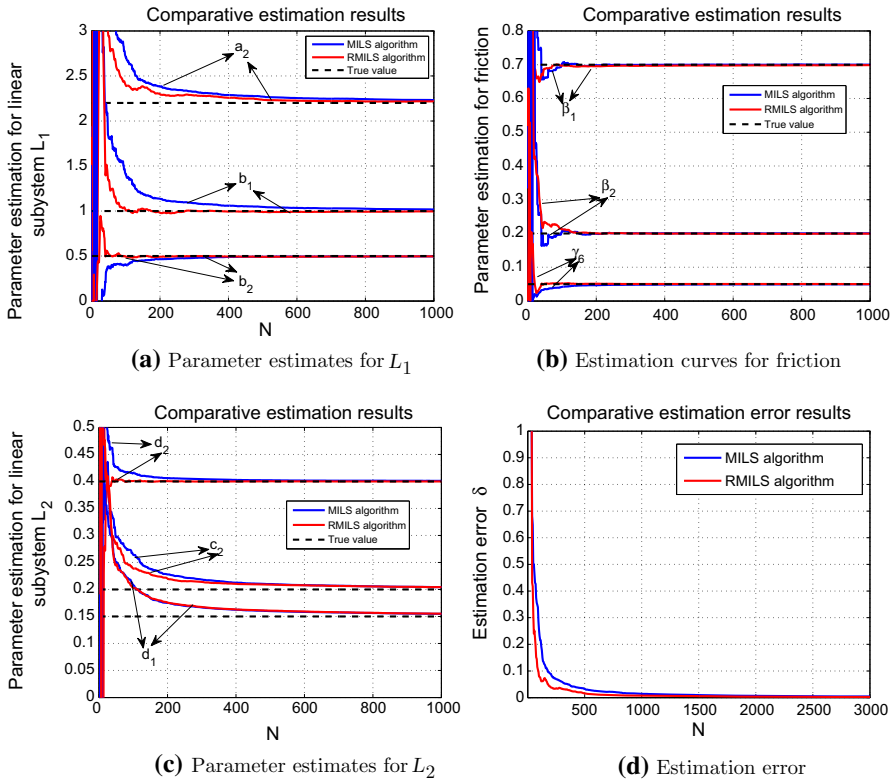**(a)** Parameter estimates for L_1

(b) Estimation curves for friction

(c) Parameter estimates for L_2

(d) Estimation error

Fig. 2 Estimation curves by both identification methods

(a) Validation for RMILS algorithm

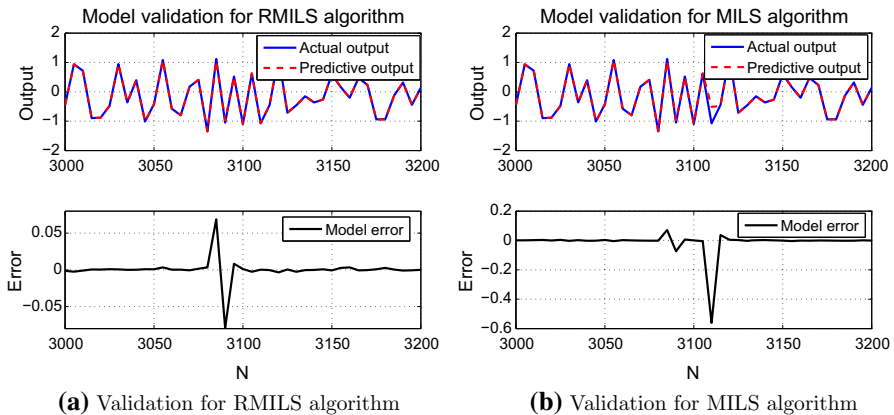**(b)** Validation for MILS algorithm

Fig. 3 Model validation for both algorithms

algorithms, it is clear that the indices are small values, which indicate that the identification algorithms produce accurate parameter estimation. Table 1 also shows that the performance of the RMILS method outperforms that of the MILS approach.

Table 1 Performance indices of the identification algorithms

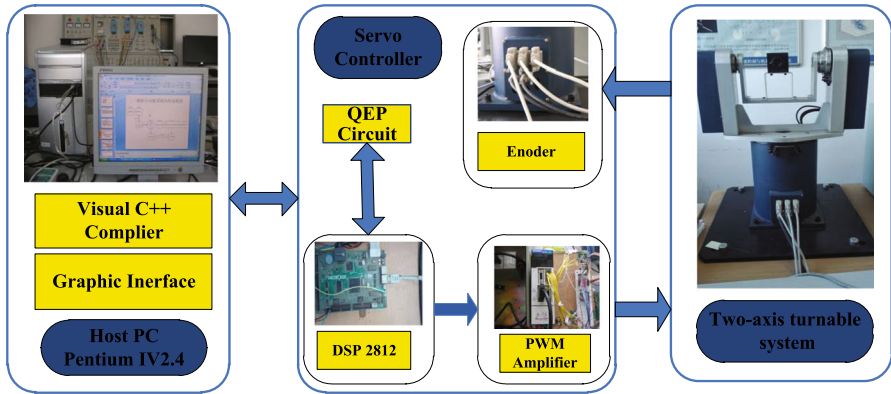| Algorithm	μ_e	e_{RMSe}	NMSE
MILS	1.6550×10^{-2}	5.9980×10^{-2}	5.9515×10^{-3}
RMILS	1.5282×10^{-4}	2.2284×10^{-3}	8.6324×10^{-5}

Fig. 4 Turntable servo system

5.2 Application

From the simulation results, it can be seen that the proposed algorithm has certain advantages in convergence speed and estimation accuracy compared to the MILS. To confirm the usefulness of the presented estimator, the RMILS is utilized to model the turntable servo system based on the W–H–S with friction. A turntable system is used as a test rig, which is depicted in Fig. 4. In this experimental platform, the stabilized platform and motor can be considered as dynamic subsystems, respectively. Friction lies in the stabilized platform and motor. To make a long story short, the turntable servo system is a W–H–S with friction system. We can use the W–H–S with friction to model the turntable system. In this rig, the motion of x-axis (or y-axis) is driven by a permanent magnet synchronous motor (HC-UFS13). A digital signal processor (TMS3202812) is used as the controller and motor drive card (MR-J2S-10A) performing as the driver, resolution of the encoder is 800 divisions. The results of the experiment are displayed on a PC Pentium 2.8 GHz.

Based on the structure of the turntable system, the Wiener–Hammerstein model can be written as follows:

(1) Linear submodel L_1 for the motor system: $x(t) = u(t-1) + A_2u(t-2) - B_1x(t-1) - B_2x(t-2)$,
(2) friction model $f(\cdot)$ for the actual nonlinearity: $v(t) = \alpha_1x(t) - \alpha_1x(t-1) + \alpha_2\text{sign}(x(t) - x(t-1)) - \alpha_3\tanh(x(t) - x(t-1))$,
(3) linear submodel L_2 for the stabilized platform (Load): $y(t) = v(t-1) + C_2v(t-2) - D_1y(t-1) - D_2y(t-2)$.

(a) Estimation curves for L_1 Submodel

(b) Parameter estimates for friction submodel

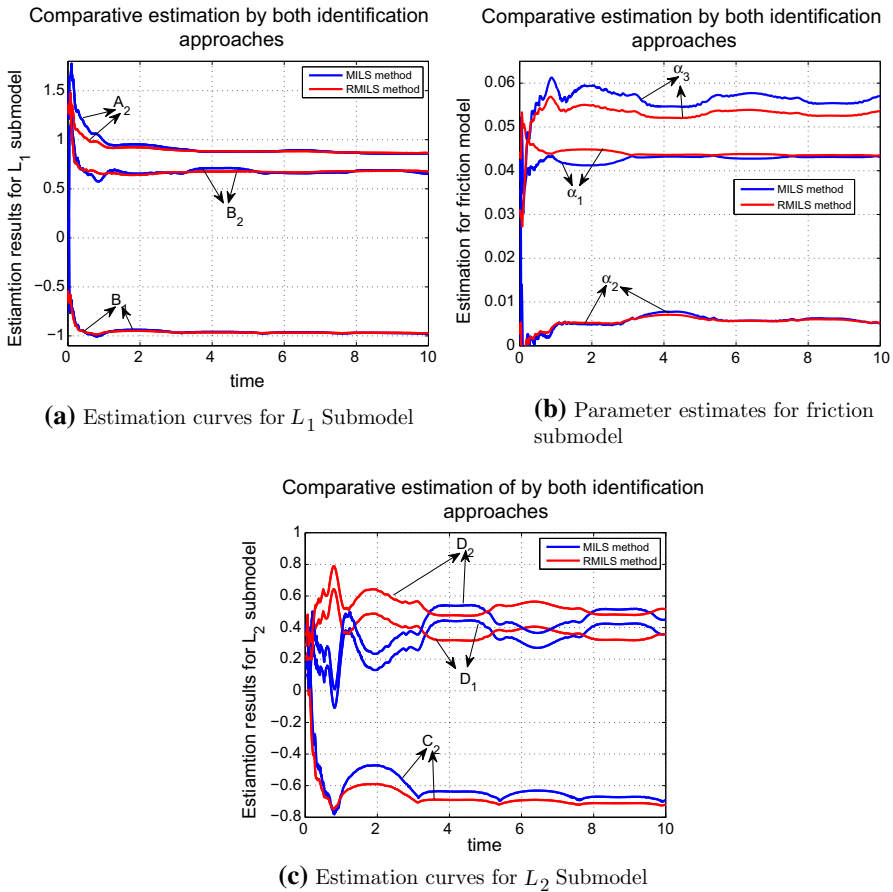**(c)** Estimation curves for L_2 Submodel

Fig. 5 Comparative estimations by both approaches

In this experiment, a PID algorithm is employed as the controller, whose parameters are chosen as $k_p = 40, k_i = 0.001, k_d = 0.2$. The reference signal $y_d = 0.8 \sin(2/5\pi t)$ is taken as the input signal. The sampling rate is 0.01 s. The initial value of θ is $\theta_0 = [0.04, 0.06, 0.044, 0.0058, 0.001, 0.036, 0.001, 0.11, 0.01]^T$, the innovation length $p = 4$, the covariance matrix is $P = 10^6 I$.

The contrastive parameter identification profiles by MILS and RMILS algorithms are plotted in Fig. 5, respectively. We can find that the estimated parameters have oscillations in the initial stage of parameter estimation by both identification schemes, but the estimated values can give close to steady values with the increase in time. The proposed approach provides smaller oscillation and faster convergence speed than the MILS algorithm. According to Fig. 5, we can obtain the corresponding estimated values $\hat{A}_2 = 0.8545$, $\hat{B}_1 = -0.9703$, $\hat{B}_2 = 0.6861$, $\hat{\alpha}_1 = 0.0436$, $\hat{\alpha}_2 = 0.006$, $\hat{\alpha}_3 = 0.0532$, $\hat{C}_2 = -0.7049$, $\hat{D}_1 = 0.3246$ and $\hat{D}_2 = 0.4869$.

To illustrate the superiority of the RMILS scheme, Fig. 6 shows the tracking outputs and errors for both algorithms based on the estimation results. It can be clearly observed
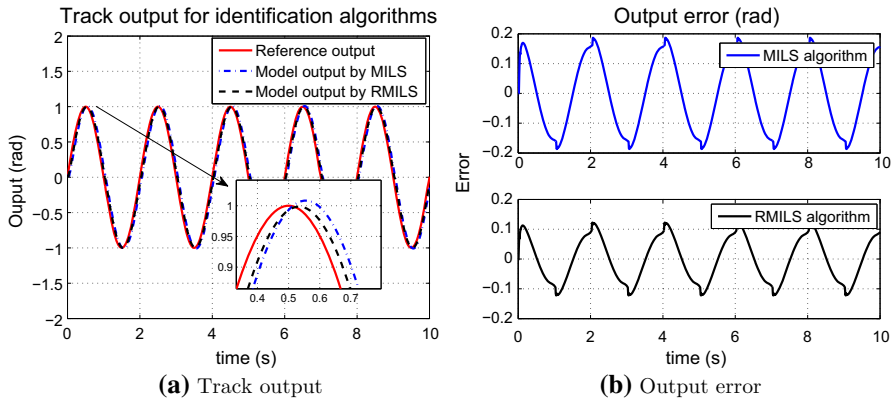
Fig. 6 Track output and error by both approaches

Table 2 Comparison of output error indices

Algorithm	μ_e	e_{RMSe}	NMSE
MILS	-6.7508×10^{-5}	3.4426×10^{-2}	2.3675×10^{-3}
RMILS	-3.9563×10^{-5}	1.3820×10^{-2}	3.8107×10^{-4}

that the obtained model outputs can track the reference output and the presented scheme produces a classy tracking performance compared with the MILS algorithm. Tracking output results indicate that the W–H-S with friction can model for the turntable servo system, and also demonstrate the advantage of RMILS. Table 2 summarizes the model error indices comparisons between the RMILS scheme and MILS algorithm. It is obvious that the developed method can give more accurate modeling results by the values of μ_e, e_{RMSe} and NMSE.

6 Discussion

Compared with our previous work in [13], this paper has the following differences. Firstly, the purpose and system characteristics of the paper are different: The publication in [13] considers the parameter estimation of the Wiener–Hammerstein systems with backlash in which backlash is a piecewise nonlinearity. However, in this paper, we use the Wiener–Hammerstein with friction to model the turntable servo system in which friction is a newly proposed continuously differentiable nonlinearity and apply the actual data of turntable servo system to identify the parameters of Wiener–Hammerstein model rather than the simulated data in [13]. Secondly, the starting point for improving the algorithm is different: In our previous work [13], which is used to improve the multi-innovation length problem for gradient method, estimator type is gradient-type method. While the identifier is least-squares-type algorithm in this paper, which is applied to address the inversion of covariance matrix for least-squares algorithm,

7 Conclusion

In this paper, a RMILS approach of estimating and modeling the Wiener–Hammerstein systems with friction nonlinearity has been proposed through the usage of the multi-step updating. To obtain the identification model of the modeling turntable servo system, the key-term separation principle is employed to address the W–H model. The components of the turntable servo system can be described by the corresponding parts of the W–H model. Then, the RMILS scheme is proposed to estimate the parameters of this model based on the system data of turntable system. By decomposing the multi-innovation into p sub-innovations, the RMILS algorithm can effectively handle the problem for the inversion of covariance matrix. Compared with the MILS algorithm, example and experiment results indicate the superiority of the proposed approach in this paper.

References

1. J. Chen, X. Wang, Identification of Hammerstein systems with continuous nonlinearity. Inf. Process. Lett. **115**, 822–827 (2015)
2. R. Dong, Y. Tan, Y. Xie, Identification of micropositioning stage with piezoelectric actuators. Mech. Syst. Signal Process. **75**, 618–630 (2016)
3. V. Filipovic, Recursive identification of block-oriented nonlinear systems in the presence of outliers. J. Process Control **78**, 1–12 (2019)
4. M. Gan, X. Chen, F. Ding, G. Chen, C.L.P. Chen, Adaptive RBF-AR models based on multi-innovation least squares method. IEEE Signal Process. Lett. **26**, 1182–1186 (2019)
5. M. Gilson, J.S. Welsh, H. Garnier, A frequency localizing basis function-based IV method for wideband system identification. IEEE Trans. Control Syst. Technol. **26**, 329–335 (2018)
6. G. Giordano, S. Gros, J. Sjöberg, An improved method for Wiener–Hammerstein system identification based on the fractional approach. Automatica **94**, 349–360 (2018)
7. G. Goodwin, K. Sin, *Adaptive Filtering Prediction and Control* (Prentice Hall, Englewood Clifs, 1984)
8. M. Han, S. Zhang, M. Xu, T. Qiu, N. Wang, Multivariate chaotic time series online prediction based on improved kernel recursive least squares algorithm. IEEE Trans. Cybern. **49**, 1160–1172 (2019)
9. K. Kostoglou, R. Schondorf, G.D. Mitsis, Modeling of multiple-input, time-varying systems with recursively estimated basis expansions. Signal Process. **155**, 287–300 (2019)
10. L. Lennart, *System Identification: Theory for the User*, 2nd edn. (PTR Prentice Hall, Upper Saddle River, 1999)
11. L. Li, X. Ren, Decomposition-based recursive least-squares parameter estimation algorithm for Wiener–Hammerstein systems with dead-zone nonlinearity. Int. J. Syst. Sci. **48**, 2405–2414 (2017)
12. L. Li, X. Ren, Identification of nonlinear Wiener–Hammerstein systems by a novel adaptive algorithm based on cost function framework. ISA Trans. **80**, 146–159 (2018)
13. L. Li, X. Ren, F. Guo, Modified multi-innovation stochastic gradient algorithm for Wiener–Hammerstein systems with backlash. J. Frankl. Inst. **355**, 4050–4075 (2018)
14. Z. Liu, X. Dang, B. Jing, A novel open circuit voltage based state of charge estimation for lithium-ion battery by multi-innovation Kalman filter. IEEE Access **7**, 49432–49447 (2019)
15. Q. Liu, F. Ding, Auxiliary model-based recursive generalized least squares algorithm for multivariate output-error autoregressive systems using the data filtering. Circuits Syst. Signal Process. **38**, 590–610 (2019)
16. Q. Liu, F. Ding, Y. Wang, T. Hayatc, Auxiliary model based recursive generalized least squares identification algorithm for multivariate output-error autoregressive systems using the decomposition technique. J. Frankl. Inst. **355**, 7643–7663 (2018)

17. L. Liu, F. Ding, C. Wang, A. Alsaedi, T. Hayat, Maximum likelihood multi-innovation stochastic gradient estimation for multivariate equation-error systems. Int. J. Control Autom. Syst. **16**, 2528–2537 (2018)
18. J. Liu, S. Kumar, D.P. Palomar, Parameter estimation of heavy-tailed ar model with missing data via stochastic EM. IEEE Trans. Signal Process. **67**, 2159–2172 (2019)
19. C. Makkar, G. Hu, W.G. Sawyer, W.E. Dixon, Lyapunov-based tracking control in the presence of uncertain nonlinear parameterizable friction. IEEE Trans. Autom. Control **52**, 1988–1994 (2007)
20. G. Mzyk, P. Wachel, Kernel-based identification of Wiener–Hammerstein system. Automatica **83**, 275–281 (2017)
21. J. Na, Q. Chen, X. Ren, Y. Guo, Adaptive prescribed performance motion control of servo mechanisms with friction compensation. IEEE Trans. Ind. Electron. **61**, 486–494 (2014)
22. J. Na, G. Herrmann, X. Ren, Neural network control of nonlinear time-delay system with unknown dead-zone and its application to a robotic servo system, in *2010 FIRA RoboWorld Congress* (Springer, Berlin, 2010), pp. 338–345
23. M. Schoukens, R. Pintelon, Y. Rolain, Identification of Wiener–Hammerstein systems by a nonparametric separation of the best linear approximation. Automatica **50**, 628–634 (2014)
24. Y. Shekofteh, S. Jafari, K. Rajagopal, V. Pham, Parameter identification of chaotic systems using a modified cost function including static and dynamic information of attractors in the state space. Circuits Syst. Signal Process. **38**, 2039–2054 (2019)
25. Q. Shen, J. Chen, X. Ma, Multi-innovation stochastic gradient algorithms for input nonlinear time-varying systems based on the line search strategy. Circuits Syst. Signal Process. **38**, 2023–2038 (2019)
26. K. Tiels, M. Schoukens, J. Schoukens, Initial estimates for Wiener–Hammerstein models using phase-coupled multisines. Automatica **60**, 201–209 (2015)
27. J. Vörös, Identification of nonlinear cascade systems with output hysteresis based on the key term separation principle. Appl. Math. Model. **39**, 5531–5539 (2015)
28. L. Wan, F. Ding, Decomposition- and gradient-based iterative identification algorithms for multivariable systems using the multi-innovation theory. Circuits Syst. Signal Process. **38**, 2971–2991 (2019)
29. S. Wang, H. Yu, J. Yu, Robust adaptive tracking control for servo mechanisms with continuous friction compensation. Control Eng. Pract. **87**, 76–82 (2019)
30. Y. Xie, Y. Tan, R. Dong, Nonlinear modeling and decoupling control of XY micropositioning stages with piezoelectric actuators. IEEE/ASME Trans. Mechatron. **18**, 821–832 (2013)
31. Q. Zhang, Q. Wang, G. Li, Nonlinear modeling and predictive functional control of Hammerstein system with application to the turntable servo system. Mech. Syst. Signal Process. **72**, 383–394 (2016)
32. Q. Zhang, Q.J. Wang, G.L. Li, Switched system identification based on the constrained multi-objective optimization problem with application to the servo turntable. Int. J. Control Autom. Syst. **14**, 1153–1159 (2016)
33. L. Zhou, X. Li, H. Xu, P. Zhu, Multi-innovation stochastic gradient method for harmonic modelling of power signals. IET Signal Process. **10**, 737–742 (2016)
34. Z. Zhou, Y. Tan, Y. Xie, R. Dong, State estimation of a compound non-smooth sandwich system with backlash and dead zone. Mech. Syst. Signal Process. **83**, 439–449 (2017)